Two distinct profiles of fMRI and neurophysiological activity elicited by acetylcholine in visual cortex

Daniel Zaldivar[a,1,2], Alexander Rauch[a], Nikos K. Logothetis[a,b], and Jozien Goense[a,c]

[a]Department Physiology of Cognitive Processes, Max Planck Institute for Biological Cybernetics, D-72076 Tübingen, Germany; [b]Centre for Imaging Sciences, University of Manchester, M13 9PT Manchester, United Kingdom; and [c]Institute of Neuroscience and Psychology, School of Psychology, University of Glasgow, G12 8QB Glasgow, United Kingdom

Edited by Marcus E. Raichle, Washington University in St. Louis, St. Louis, MO, and approved November 6, 2018 (received for review May 18, 2018)

Cholinergic neuromodulation is involved in all aspects of sensory processing and is crucial for processes such as attention, learning and memory, etc. However, despite the known roles of acetylcholine (ACh), we still do not how to disentangle ACh contributions from sensory or task-evoked changes in functional magnetic resonance imaging (fMRI). Here, we investigated the effects of local injection of ACh on fMRI and neural signals in the primary visual cortex (V1) of anesthetized macaques by combining pharmaco-based MRI (phMRI) with electrophysiological recordings, using single electrodes and electrode arrays. We found that local injection of ACh elicited two distinct profiles of fMRI and neurophysiological activity, depending on the distance from the injector. Near the injection site, we observed an increase in the baseline blood oxygen-level-dependent (BOLD) and cerebral blood flow (CBF) responses, while their visual modulation decreased. In contrast, further from the injection site, we observed an increase in the visually induced BOLD and CBF modulation without changes in baseline. Neurophysiological recordings suggest that the spatial correspondence between fMRI responses and neural activity does not change in the gamma, high-gamma, and multiunit activity (MUA) bands. The results near the injection site suggest increased inhibitory drive and decreased metabolism, contrasting to the far region. These changes are thought to reflect the kinetics of ACh and its metabolism to choline.

BOLD-fMRI | CBF-fMRI | nonhuman primate | electrophysiology | visual cortex

The interpretation of functional magnetic resonance imaging (fMRI) studies requires understanding the quantitative relationship between the blood oxygen-level-dependent (BOLD) signal changes and their underlying electrophysiological activity. Several studies have focused on understanding the nature of electrophysiological signals [spikes vs. local field potentials (LFPs)] driving the fMRI signal and have confirmed that fMRI responses are generally reliable indicators of neural activity (1–5). However, it has also been shown that the relation between neural activity and fMRI responses can change in different cognitive states (6, 7). These cognitive states are mediated by diverse neuromodulators that enable transitions from one brain state to another on a variety of time scales (8, 9). Neuromodulators can change the input–output relationship of neural circuits, either locally or on a global scale, and adjust their energy expenditure, and thereby they also affect the hemodynamic responses and fMRI signals (2, 8, 10, 11). However, it is unclear how to interpret the effects of neuromodulation in fMRI signals, for instance, how to disentangle the BOLD signal changes relating to task or attention (presumably under neuromodulatory influence; ref. 12) from stimulus-driven or perceptual effects. Understanding how neuromodulators affect the BOLD responses is essential for the effective interpretation of fMRI data, not only in tasks involving attentional processes, but also for potential diagnostic use of fMRI, since many neurological and psychiatric disorders lead to alterations in neuromodulatory systems (13).

Acetylcholine (ACh) is a key neuromodulator in the brain and is involved in many aspects of cognition, including sensory processing (14–16), attention (14), and learning and memory (17). Nearly all cortical regions receive cholinergic projections that originate from the basal forebrain (BFB; ref. 18), and histological evidence has shown differential distributions of cholinergic receptors (AChRs; refs. 19, 20) and acetylcholinesterase (AChE) in cortex (21). However, despite this anatomical evidence, it has generally been assumed that the cholinergic system exerts uniform effects across all cortical structures (22).

Studies using electrical microstimulation of BFB neurons (16, 22) and systemic injection of cholinergic agonists (23) have shown increases in sensory-evoked neural activity in visual cortex as well as in cerebral blood flow (CBF; refs. 22–25). This effect of ACh has also been observed in other sensory modalities, such as the somatosensory (26) and the auditory cortices (27). However, it is unclear to what extent these changes are the result from local cholinergic effects or caused by a chain of events instantiated by global changes in ACh levels (28).

In this study, we combined intracortical injections of ACh with pharmaco-MRI (BOLD and CBF) and electrophysiology [single-electrode physiology and microelectrocorticography (μECoG) electrode arrays] to investigate the impact of cholinergic neuromodulation on neural responses and neurovascular coupling in macaque V1. Applying ACh in anesthetized animals allowed us to investigate the mechanisms by which ACh affects neural and fMRI responses without the potentially confusing effects of

Significance

fMRI changes are typically assumed to be due to changes in neural activity, although whether this remains valid under the influence of neuromodulators is relatively unknown. Here, we found evidence that intracortical acetylcholine elicits distinct profiles of fMRI and electrophysiological activity in visual cortex. Two patterns of cholinergic activity were observed, depending on the distance to the injection site, although neurovascular coupling was preserved. Our results illustrate the effects of neuromodulators on fMRI and electrophysiological responses and show that these depend on neuromodulator concentration and kinetics.

Author contributions: D.Z., A.R., and N.K.L. designed research; D.Z., A.R., and J.G. performed research; D.Z., N.K.L., and J.G. contributed new reagents/analytic tools; D.Z. analyzed data; D.Z. and J.G. wrote the paper; and N.K.L. and J.G. supervised the research.

The authors declare no conflict of interest.

This article is a PNAS Direct Submission.

[1]To whom correspondence should be addressed. Email: Daniel.Zaldivar@tuebingen.mpg.de.

[2]Present address: Section on Cognitive Neurophysiology and Imaging, National Institute of Mental Health, Bethesda, MD 20892.

This article contains supporting information online at www.pnas.org/lookup/suppl/doi:10.1073/pnas.1808507115/-/DCSupplemental.

Published online December 3, 2018.

behavioral processes like attention (15) or learning (29). We found two distinct cholinergically induced effects in the fMRI and neurophysiological responses in V1. Near the injection site, the amplitude of the BOLD, CBF, and neural responses to the visual stimulus was decreased and the baseline increased. Further away from the injection site, visually induced modulation of the BOLD, CBF, and neural responses increased, with no changes in the baseline, and preserved neurovascular coupling.

Results

Our goal was to investigate the effects of cholinergic neuromodulation on neurovascular coupling. For this, we combined functional imaging in V1 with neurophysiology and pharmacology in anesthetized nonhuman primates (*Macaca mulatta*). We acquired BOLD, functional CBF (fCBF), and neurophysiological data, the latter using single electrodes as well as μECoG arrays, while animals viewed a rotating checkerboard (Fig. 1 *A* and *B*). We mimicked cholinergic neuromodulation by locally applying ACh in V1. To ensure that ACh was reliably delivered, we monitored the changes in the concentration of ACh in the extracellular space using microsampling in conjunction with HPLC coupled to mass spectrometry (*SI Appendix*, Fig. S1). Following the injection of ACh, we found that levels of ACh immediately increased from baseline levels and returned to baseline levels 10 min after the end of the injection (*SI Appendix*, Fig. S1*B*).

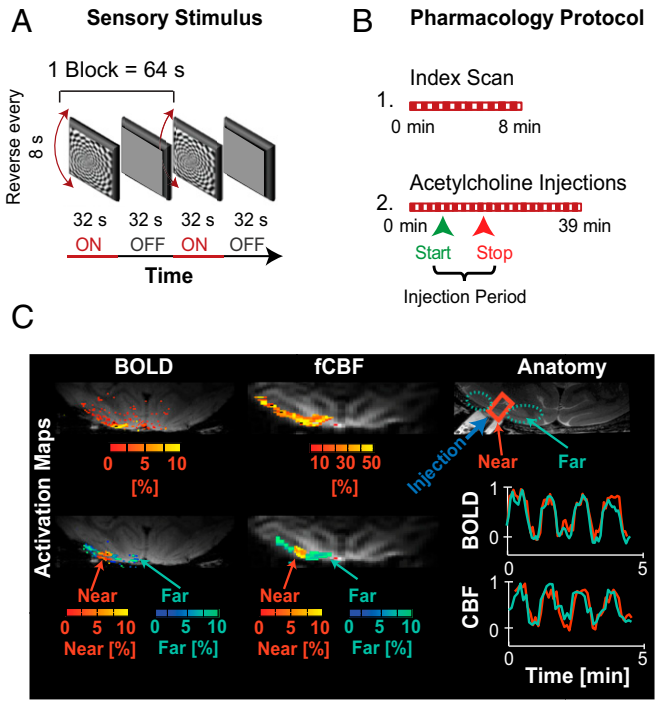

Fig. 1. Experimental paradigm and representative example of an experimental session showing functional activation maps for BOLD and CBF. (*A*) Experimental paradigm and design. The stimulus paradigm consisted of blocks of a rotating polar black-and-white checkerboard of 32 s intervened by a black screen of equal duration. (*B*) Every experiment was divided in two sessions: an 8-min scan without pharmacological intervention to define the ROIs (*B1*); and a longer scan consisting of 37 stimulus repetitions during which local cholinergic injection took place (*B2*). The start of the injection was at 4 min (fourth repetition), and the injection finished at 8.5 min (end of eighth repetition). (*C*) Functional activation maps of voxels that showed a significant response to the visual stimulus. *C*, *Upper* represents the activation in V1 (E04.S91). (*C*, *Left Upper*) Activation map for BOLD: FOV 6.4 × 4.8 mm^2. (*C*, *Center Upper*) CBF, FOV, 64 × 64 mm^2. (*C*, *Left* and *Center Lower*) The BOLD and CBF time courses of the activation in two ROIs: These two ROIs were defined based on the location of the injector (blue arrow): Near corresponds to voxels near the injector (red arrow), and Far corresponds to voxels far from the injection site (3–5 mm, green arrow).

ACh Alters Sensory Evoked Neural Activity in Primary Visual Cortex. We first investigated the effects of ACh on neural activity, because studies have shown that at the neural population level, ACh reduces excitability (30–33). We were interested to know if our pharmacological approach yielded similar results to those reported. We used neurophysiology data that was simultaneously collected with fMRI data and calculated the absolute power spectral density (PSD) from the LFPs and multiunit activity (MUA) using previously described methods (11, 34). Changes in the PSD are good indicators of changes in neural activity, as these reflect changes in the coordinated activity of excitatory and inhibitory postsynaptic potentials (1, 3, 5, 35, 36). Our analysis revealed that injection of ACh decreased the power of the neuronal activity across a wide frequency range (1–250 Hz; *SI Appendix*, Fig. S2). However, given that it has been shown that the gamma (γ; 50–90 Hz), high-gamma (hγ; 91–150 Hz), and MUA (900–3,000 Hz) bands carry most information about the sensory stimulus and are most strongly correlated with the fMRI signal (4, 5, 37), we focused our analysis on these bands.

Fig. 2 illustrates the effects of ACh injection on the LFP and MUA: Fig. 2 *A*–*C* show the average time courses over 15 experimental sessions for the extracted frequency bands. The visual stimulus caused an increase in power/amplitude of >10% compared with baseline in all frequency bands. A substantial effect of the ACh injection is evident in the γ, hγ, and MUA bands (Fig. 2 *A*–*D*) as a decrease in visual modulation in the γ ($MOD_{drug,\ \gamma}$ 62 ± 2%; $P = 0.028$), in the hγ ($MOD_{drug,\ h\gamma}$ 65 ± 2%; $P = 0.031$), and in the MUA ($MOD_{drug,\ mua}$ 64 ± 1%; $P = 0.025$) bands. The effects of ACh on the γ, hγ, and MUA amplitude returned to baseline ∼22 min after the ACh infusion was stopped.

Moreover, it has been shown that ACh can affect the amplitude of the response as well as the variability of the neural activity, which impacts the information encoding in the visual cortex (8, 9, 15, 16, 38). Therefore, we calculated the signal-to-noise ratio (SNR). This showed an increase in SNR in the hγ ($SNR_{drug,\ h\gamma} = 11.5 \pm 2.4$ dB; $P = 0.031$, paired t test) and MUA ($SNR_{drug,\ MUA} = 11 \pm 2.2$ dB; $P = 0.027$, paired t test) bands starting shortly after the beginning of the injection. The SNR in the γ band was not significantly increased ($SNR_{drug,\ \gamma} = 10.4 \pm 2.8$ dB; $P = 0.59$, paired t test). None of these effects were observed during control injection of artificial cerebrospinal fluid (ACSF; see *SI Appendix*, Figs. S2 and S3).

Evoked BOLD Responses Under Cholinergic Influence. The neural data in Fig. 2 were recorded simultaneously with BOLD responses. Fig. 3*A* shows an example of a typical functional activation map showing the selected V1 regions before and during injection of ACh. We selected two regions of interest (ROIs) (Fig. 1*C*) according to their location relative to the injector: ROI_{NEAR} (voxels located within a ∼2-mm diameter surrounding the electrode) and ROI_{FAR} (voxels located further away from the injector, 3–5 mm). These criteria led us to identify two distinct effects of ACh in the BOLD signal. The average visually induced BOLD change in V1 was 5.8 ± 0.25% (15 experimental sessions) in both ROIs. The activated voxels in both selected regions are color-coded according to their percentage changes (Fig. 3*A*) and location in the near or far ROI. Fig. 3 *B* and *C* show the time courses of the response of the BOLD modulation over the course of the ACh injection in both ROIs. The time course for the voxels in the ROI_{NEAR} ($BOLD_{NEAR}$; red) exhibited an increase in the baseline following the start of the injection, which reached its maximum ∼2 min after the start of the injection (Fig. 3*B*). In contrast, the time course of the ROI_{FAR} (Fig. 3*C*, $BOLD_{FAR}$) did not show this shift in the baseline and remained stable throughout the experiment. ACh also elicited different

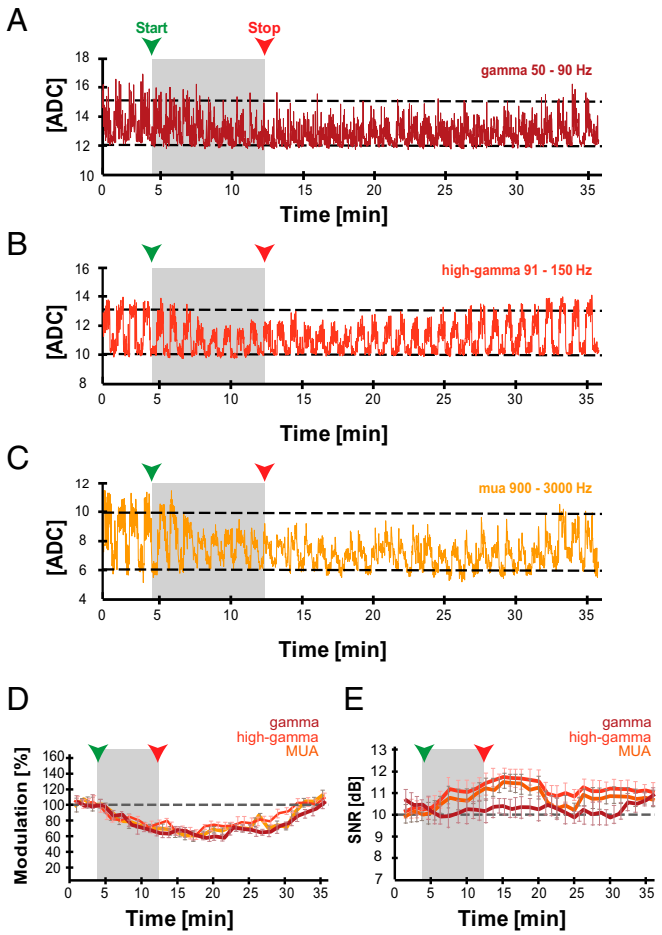

Fig. 2. Local application of ACh decreases the power in LFP and MUA bands. The average time course of the neural activity (γ, hγ, and MUA bands) across experiments in response to ACh injection (n = 15 sessions) is shown. The green and red arrows indicate the beginning and end of the injection of ACh (shaded gray area). (*A*) The γ band (50–90 Hz). (*B*) The hγ band (91–150 Hz). (*C*) MUA band (900–3,000 Hz). In all bands, the amplitude of the visual response decreased following the injection of ACh, while the variability decreased in the hγ and MUA bands, but not in the γ band. (*D*) Percentage changes in visual response of γ, hγ, and MUA. (*E*) The SNR of the hγ and MUA increases upon ACh infusion, as a result of decreased variability.

effects on the visually induced modulation in the "near" and "far" regions. The visual modulation in the $BOLD_{NEAR}$ decreased, while the $BOLD_{FAR}$ modulation increased (Fig. 3 *B* and *C*, respectively). To quantify the effects of ACh on the evoked BOLD responses, we analyzed the modulation in response to visual stimulation normalized to the predrug condition (Fig. 3 *D* and *E*). During the drug infusion, the mean $BOLD_{NEAR}$ exhibited a significant reduction in the modulation compared with the predrug condition ($MOD_{drug,\ NEAR}$ 48 ± 3%; P = 0.032, paired t test; Fig. 3*D*, shown in red). In contrast, the mean $BOLD_{FAR}$ showed a significant increase in the amplitude of visually evoked responses ($MOD_{drug,\ FAR}$ 133 ± 4%; P = 0.036, paired t test; Fig. 3*D*, shown in teal). To get a better intuition about the effects elicited by the ACh injection, we also computed baseline changes—that is, the image intensity in the periods without visual stimulation (Fig. 3*E*). We found that mean $BOLD_{NEAR}$ exhibited a substantial increase in its baseline ($BOLD_{drug,\ NEAR}$ 136 ± 3%; P = 0.025, paired t test), while the baseline did not change for $BOLD_{FAR}$. None of these changes were observed during control injections of ACSF (*SI Appendix*, Fig. S3).

Evoked CBF Responses Under Cholinergic Influence. The BOLD signal reflects the deoxyhemoglobin concentration [dHb] and thus is affected by changes in the cerebral blood volume (CBV), CBF, and cerebral metabolic rate of oxygen consumption ($CMRO_2$). In earlier work, we showed that these fMRI signals were differentially affected by dopamine (10) and found that BOLD-fMRI alone cannot be used to make inferences about changes in neural activity and metabolism under neuromodulation. Following this line of argument, we performed CBF measurements using the same pharmacological approach. Using arterial spin labeling (ASL) in combination with BOLD-fMRI and electrophysiology may offer better insights into the changes in energy metabolism following changes in neural activity. Fig. 4*A* shows activation patterns of the CBF in V1 before and during injection of ACh. As for the BOLD responses, we generated two ROIs relative to the location of the injector and computed the visually induced modulation and baseline changes. The mean CBF change in the ROIs was 36 ± 2.1% (seven experimental sessions), in line with earlier CBF changes in anesthetized monkeys V1 (39–41). The average time course of the CBF_{NEAR} across experiments (Fig. 4*B*) showed a positive shift in the baseline and a decrease in visually induced modulation similar to the changes in the BOLD activity. When comparing the CBF_{NEAR} "predrug" period with the "drug" period, we observed a mean decrease in the visually induced modulation ($CBF_{drug,\ NEAR}$ = 65 ± 5%; P = 0.043, paired t test, n = 7). The largest CBF decrease was observed toward the end of the infusion (62% at ∼8 min after the start of the infusion; Fig. 4*D*). The increase in the baseline started ∼1.5 min after the onset of the injection ($CBF_{drug,\ NEAR}$ = 118 ± 4%; P = 0.038, paired t test). In contrast, the CBF_{FAR} showed a mean increase in the visually induced modulation ($CBF_{drug,\ FAR}$ = 123 ± 5%; P = 0.042, paired t test) and no changes in the baseline (Fig. 4 *D* and *E*), similar to those reported for BOLD. To summarize, the CBF experiments also revealed two distinct changes in the CBF responses and mirrored the BOLD and neural responses. An increase of the baseline and a decrease in visually evoked modulation was observed in the CBF_{NEAR}, whereas we observed an increase in the visually induced modulation and no changes in the baseline for CBF_{FAR}.

ACh Does Not Change the Correspondence Between Neural Activity and fMRI Responses. An important question was to establish whether the two distinct cholinergically induced profiles of fMRI activity, in the different spatial regions, corresponded with the local neural activity. To record neural responses over an area corresponding to the extent of the fMRI responses, we acutely implanted μECoG arrays on the surface of the brain (Fig. 5*A*, μECoG 32 channels). We selected the electrode contacts according to the following criteria: (*i*) electrodes that were located within a 1-mm ratio close to the injector were assigned as $ECoG_{NEAR}$ (Fig. 5*A*, shown in red); (*ii*) electrodes that were within a ratio of 1.5–2.5 mm were assigned as $ECoG_{FAR}$ (Fig. 5*A*, shown in teal); and (*iii*) electrodes that were located on top of a blood vessel were not considered in the analysis. We first determined if there were differences between the LFP power in the two regions by computing the strength of the oscillatory activity across electrodes in $ECoG_{NEAR}$ and $ECoG_{FAR}$. Fig. 5*B* denotes a typical average LFP spectrum in V1 over electrode sites located in $ECoG_{NEAR}$ (six experimental sessions) and electrode sites in $ECoG_{FAR}$, shown in red and teal, respectively. Similar to what we observed during single-electrode recordings, the broadband LFP power in the near region decreased following the injection of ACh (*SI Appendix*, Fig. S2, shown in red). Moreover, the power in the broadband LFP in the region far from the injector increased (*SI Appendix*, Fig. S2, shown in blue).

Fig. 5 *C*–*F* illustrates the effects of ACh on the γ LFP bands: Fig. 5 *C* and *D* shows the average time courses across experiments for the γ and hγ. We focused on the γ and hγ, given that these bands originate from different sources. For instance, γ is

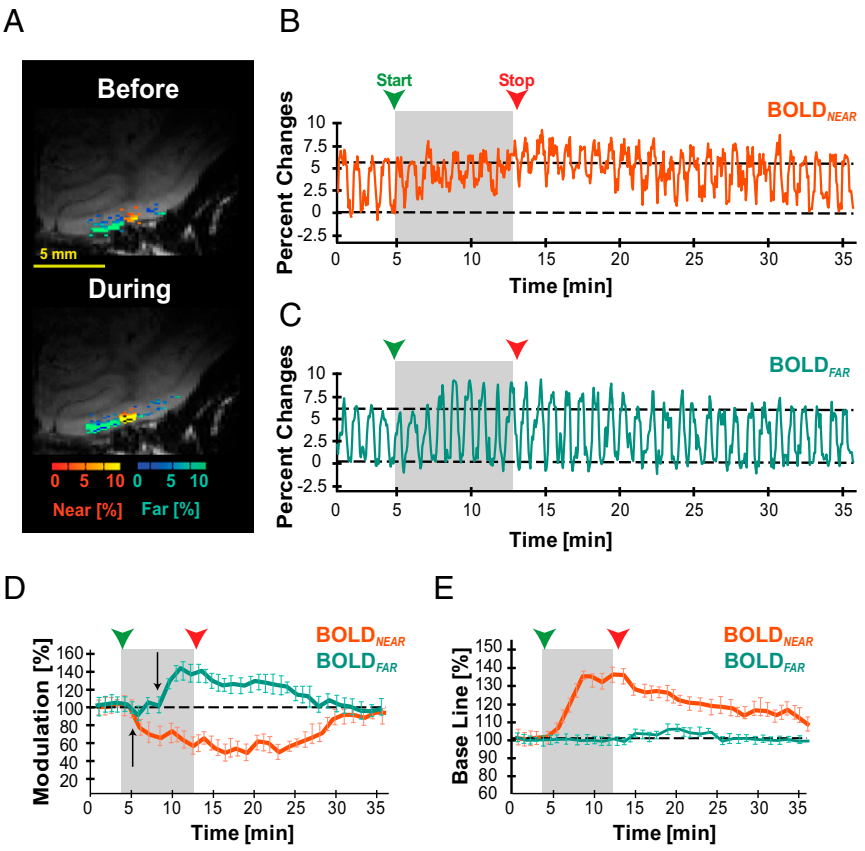

Fig. 3. ACh elicits distinct BOLD effects in regions near to and far from the injector. Mean effects of ACh injection are shown. (*A*) Activation maps of voxels responding to visual stimulation and time courses showing BOLD responses before and during the injection of ACh [monkey B05; gradient-echo (GE) echo-planar imaging (EPI) with 1-mm slice thickness]. (*B*) Time course of BOLD$_{NEAR}$ (red) response in 15 fMRI experimental sessions showed a decrease in visually induced modulation and a baseline increase following injection. (*C*) The time course of the BOLD$_{FAR}$ (green) response showed an increase in visually induced modulation without a baseline shift. (*D*) The average BOLD$_{NEAR}$ response to the visual stimulus decreased by 45% compared with the predrug period, while it increased by 43% for the BOLD$_{FAR}$. The arrows indicate the time at which the effect begins following the start of the injection. (*E*) The baseline did not change in the far region, but it increased in the near region.

closely linked to changes in excitation/inhibition balance, while the hγ has a closer relation to the MUA (42, 43). The average visually induced modulation in the γ range was increased >13% relative to the baseline. The effects of ACh on activity recorded by electrodes in ECoG$_{NEAR}$ were similar to the effects described in Fig. 2—that is, we observed that during the injection period, the visual modulation in the γ band decreased (MOD$_{\gamma,\ NEAR}$ 63 ± 3%; $P = 0.031$; Fig. 5 *C* and *E*, dark red), as well as in the hγ band (MOD$_{h\gamma,\ NEAR}$ 72 ± 4%; $P = 0.038$; Fig. 5 *C* and *E*, red). In contrast, the electrodes located in ECoG$_{FAR}$ showed an increase in the amplitude of the γ band during the injection period (MOD$_{\gamma,\ FAR}$ 123 ± 2%; $P = 0.033$; Fig. 5 *D* and *E*, blue) and hγ band (MOD$_{h\gamma,\ FAR}$ 124 ± 2%; $P = 0.038$; Fig. 5 *D* and *E*, teal). The SNR in the γ range at the ECoG$_{NEAR}$ electrodes was unaffected by the ACh injection (SNR$_{\gamma,\ NEAR}$ = 0.95 ± 0.15 dB; $P = 0.38$; Fig. 5*F*, dark red). However, the SNR in the hγ range increased (SNR$_{h\gamma,\ NEAR}$ = 1.14 ± 0.18 dB; $P = 0.033$; Fig. 5*F*, light red). The SNR of the γ band recorded by electrodes in the ECoG$_{FAR}$ region was unaffected by the injection (SNR$_{\gamma,\ FAR}$ = 0.98 ± 0.25 dB; $P = 0.33$ paired *t* test; Fig. 5*F*, dark blue), while the SNR in the hγ showed a decrease (SNR$_{h\gamma,\ FAR}$ = 0.83 ± 0.35 dB; $P = 0.031$ paired *t* test; Fig. 5*F*, green). Overall, these results reveal (*i*) a reduced neural activity at the population level (γ) in the region near the injector while neural activity was increased far from the injector; and (*ii*) a direct cholinergic influence in shaping the fidelity (SNR) of neural γ activity in the region near the injector, while fidelity appears to decrease away from the injector.

ACh Pharmacodynamics. The profiles of fMRI and neurophysiological activity described above can be caused by the effects of ACh or could be due to the influence of choline (Ch). Ch is the immediate metabolite of ACh and has been shown to activate nAChRs and to increase neural activity (44, 45). By extracting extracellular brain fluid (EBF) using microdialysis (see detailed information in *SI Appendix*; ref. 46), we simultaneously monitored how our injections influenced the concentration of Ch and ACh in the EBF in V1. We found that, following the ACh injection, the concentrations of ACh and Ch increased (*SI Appendix*, Fig. S1*B*, shown in blue and red, respectively). However, ACh and Ch exhibited different pharmacodynamics (for details, see *SI Appendix*, Fig. S1*B*).

Discussion

We used pharmaco-MRI (BOLD and CBF), neurophysiology (single-electrode recording and μECoG arrays), and intracortical injections to understand the effects of ACh on neural and fMRI activity in V1. The main finding is that the injection of ACh elicits two distinct fMRI and neural responses in V1 depending on the distance to the injector: (*i*) near the injection site, the stimulus-induced fMRI responses (BOLD and CBF) decreased with a concomitant increase in baseline activity, while the power of the neural activity decreased and its SNR increased; and (*ii*) further away from the injector we observed an increase in the visually induced modulation of the hemodynamic signals with a concomitant increase in LFP power but a decrease in the SNR of the neural activity. The decreased cell-population activity concomitant with the BOLD and CBF responses in the region near the injector might be an indication of decreased energy demands, while further away from the injector, the increased neural activity and fMRI responses might suggest increased energy demands. The increases in modulation of the hemodynamic and neural responses in the region far from the injector suggest an increased metabolic demand due to the increased neural activity, which might be due to the activation of nAChRs caused by Ch. Overall, our findings indicate that the effects of neuromodulators can vary considerably, depending on properties of local circuits and neuromodulators, such as the distance from

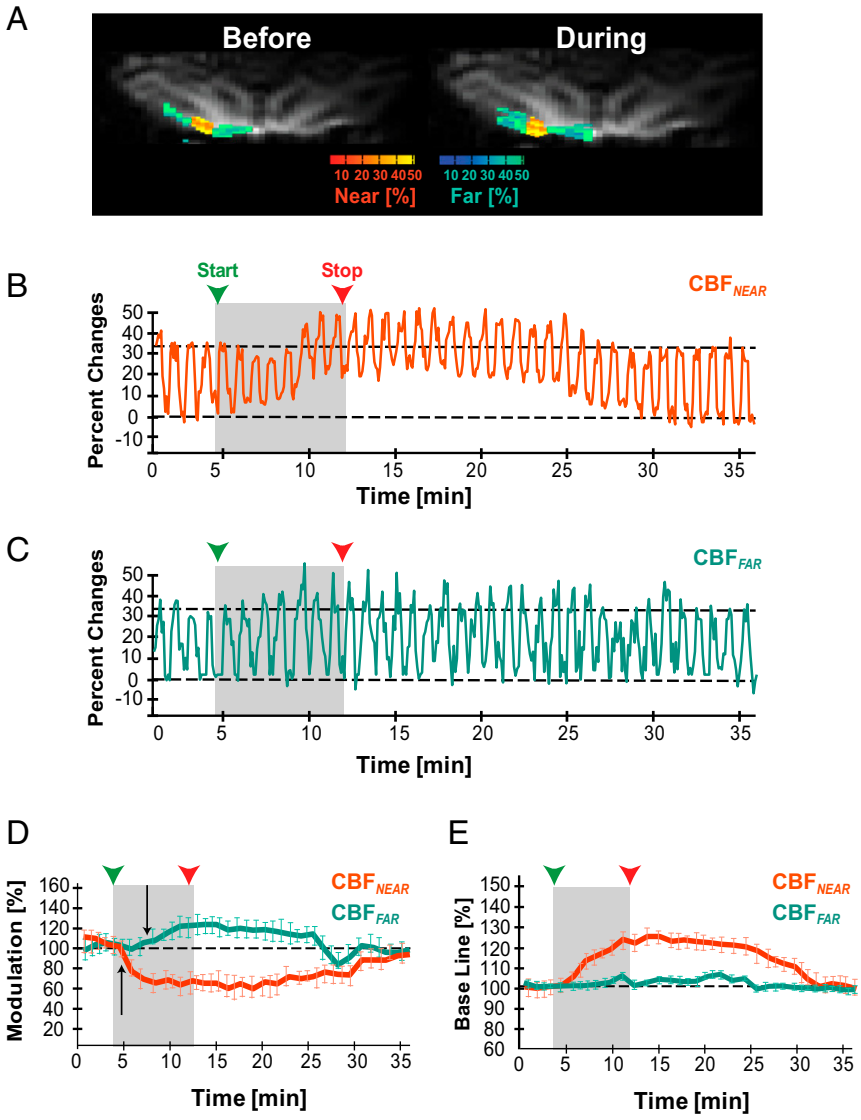

Fig. 4. CBF responses elicited by local injection of ACh. (*A*) Activation maps of FCBF in primary visual cortex (monkey E04) in response to visual stimulation and pharmacological injection. (*B* and *C*) Time course of the CBF response for the two ROIs (seven experimental sessions). (*B*) CBF_{NEAR} shows an increase in the baseline CBF and a decrease in visually induced CBF. (*C*) In contrast, the visually induced modulation in the CBF_{FAR} increased, while the baseline did not change. (*D*) The average visually induced modulation for CBF_{NEAR} and CBF_{FAR} showed a decrease (~40%) and increase (~20%), respectively, in response to ACh injection. (*E*) The baseline CBF_{NEAR} increased ~30%, whereas the baseline CBF_{FAR} did not show any changes following the injection.

release of a neuromodulator, concentration differences, and the kinetics of the neuromodulator.

Cholinergically Induced Changes in Neural Activity. ACh decreased the power in the γ, hγ, and MUA bands near the injection site. This decrease in power is in good agreement with electrophysiological studies in monkeys, which demonstrated strong inhibition of V1 activity after ACh injection (21, 32, 33). This has been ascribed to the activation of muscarinic receptors (mAChRs, particularly type 1), which are the most abundant AChRs in V1 (47) and are mostly expressed on parvalbumin-immunoreactive (PV-ir) interneurons (19, 31, 32), which in monkeys constitute 78% of the interneurons in cortex (48).

Although our results are in good agreement with findings reported in the sensory cortices of monkeys (32, 33), cats (49), and guinea pigs (50), our results contrast with evidence showing increased sensory-evoked activity in the sensory cortices of rats (22, 51, 52). A possible explanation for this discrepancy may be interspecies differences (33, 53). For instance, 25–95% of pyramidal neurons in the rodent sensory cortex are responsive to ACh, leading to an increase in neural activity (53). This neuromodulatory effect is rare in monkeys because few excitatory neurons express mAChR (19, 31). Moreover, in rat visual cortex, <50% of inhibitory neurons are PV-ir (54), and they either do not respond to (53) or are hyperpolarized by ACh (55).

The effects of ACh are multiple and complex and are ascribed to various factors, including the concentration of ACh (17, 56), the receptor types mediating cholinergic effects (15, 31, 32), and density and location of cholinergic inputs and receptors (19). We do not know for certain whether changes in network dynamics at the injection site might lead to the changes observed in the far region. Our neurophysiological recordings were collected simultaneously and from upper cortical layers, where the majority of the output and lateral connections are located. However, we believe that neural network effects are less likely to contribute to the changes in the far region, because neurons in the near and

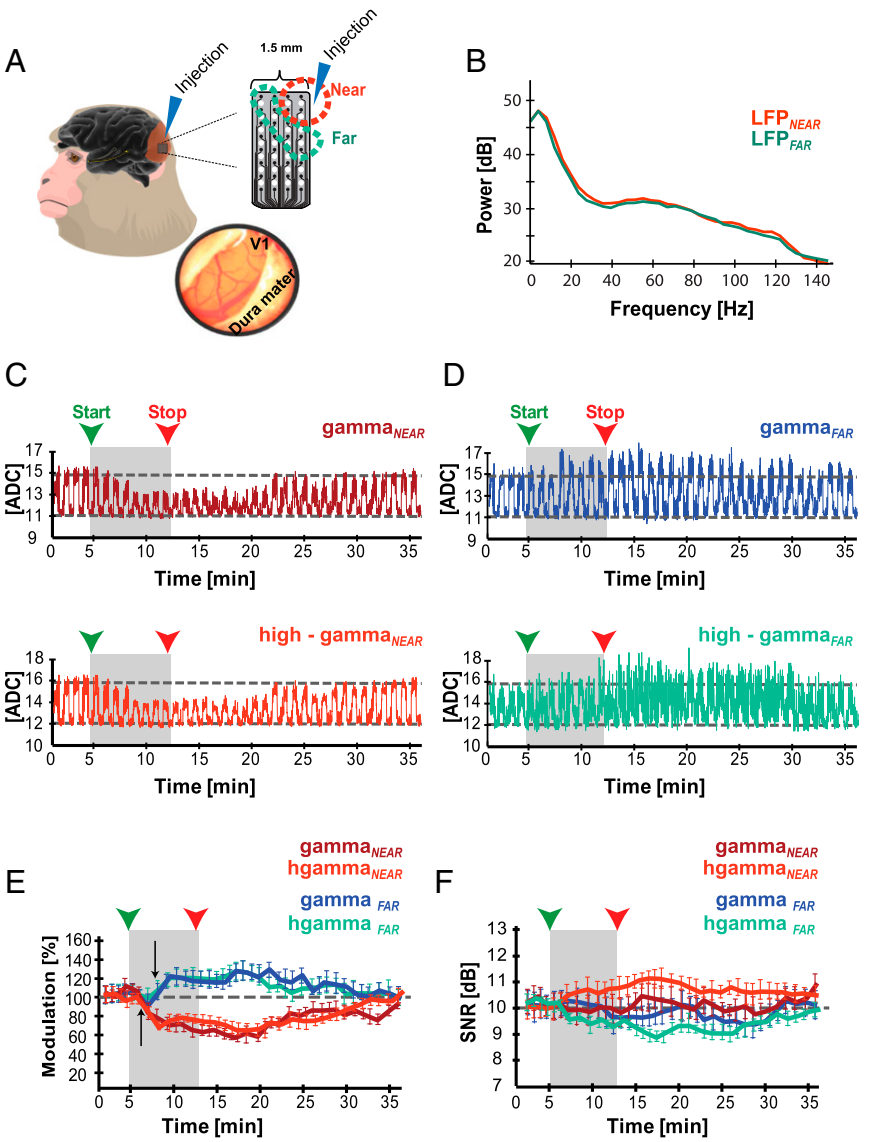

Fig. 5. The γ and hγ band activity in the near and far regions is differentially affected by ACh injection. (*A*) μECoG arrays used for this study consisted of 32 electrodes in a 4 × 8 pattern (small black dots) fabricated on a 20-μm-thick polyimide film. The arrays were positioned on the surface of the brain after carefully opening the dura mater while avoiding damage to the surface of the brain. (*B*) LFP power spectrum from the near and far regions, during the presentation of visual stimuli. (*C* and *D*) The average time course of neural activity across experiments in response to ACh injection ($n = 6$ experiments). The green and red arrows indicate the start and end of the injection (indicated by the shaded area), respectively. (*C*) The γ_{NEAR} band (50–90 Hz; dark red) and $h\gamma_{NEAR}$ (91–150 Hz, red). (*D*) The γ_{FAR} band (blue) and $h\gamma_{FAR}$ (green). (*E*) Percentage change in visual response for the γ frequency bands in the near and far regions. The electrode sites near the injector showed a decrease in amplitude of the visually induced modulation, while the electrodes far from the injector showed an increase in amplitude. (*F*) The SNR in the γ and hγ: The SNR for the near region increased in the γ and hγ bands, while the SNR in the far region decreased, in particular in the hγ band.

far region are driven by the same sensory stimulus—that is, a full-field stimulus. The neuronal activity of nearby neurons (within <2 mm) is usually synchronized, suggesting a prominent contribution from horizontal cortical connections (57). However, at larger distances, the correlation drops, reflecting a rapid spatial decay of lateral connections (57, 58). Interestingly, in vitro studies in cortical slice preparations have shown that ACh suppresses the spread of cortical excitability within a distance of <2 mm (59).

Cholinergic terminals in the cortex not only support wired neurotransmission, but also volume transmission, suggesting that ACh can influence an area beyond its site of release (60–63). Therefore, the increase in LFP power further away from the injector could be related to the diffusion of ACh from the site of injection. However, concentration differences between both regions cannot explain the distinct operational modes observed in our results because lower concentrations of ACh in the far region relative to the site of the injection would have decreased neural activity (29). In addition, the diffusion of ACh over a larger area is usually limited by AChE, which is highly expressed in cortex (21, 64). Thus, the most likely explanation of our results in the region far from the injector is that these effects are mediated by the metabolites of ACh. ACh is metabolized into Ch and acetate (65). Interestingly, studies have suggested that Ch activates nicotinic receptors (nAChRs), particularly those expressing the alpha-7 unit (44, 45, 66, 67). The activation of nAChRs is known to increase neural activity as it enhances the thalamocortical postsynaptic potentials (32, 51, 68), which in monkey V1 leads to an

increase in responsiveness and contrast sensitivity of neurons (32). In agreement with this hypothesis, our neurochemistry data show a rapid decline of ACh compared with Ch, and given the diffusion capabilities of Ch (69), we believe that the Ch-induced activation of nAChRs in the far region is the most likely scenario. However, further experiments are needed to better understand these mechanisms.

Cholinergically Induced BOLD and CBF Profiles. Neuromodulators affect the intrinsic dynamics of target neurons as well as the metabolic properties of neural circuits (8, 10, 11, 22, 70), and, in addition, they can have direct vascular effects. To better understand these different changes associated with ACh, we measured BOLD and fCBF, which reflect different aspects of the hemodynamic response (71). The BOLD signal is driven by changes in [dHb] and depends on the combined changes of CBF, CBV, and the $CMRO_2$. The CBF-based MRI signal reflects protons in arterioles and capillaries and their exchange with tissue water. In agreement with our neurophysiology results, we found two distinct cholinergically induced profiles in the BOLD and CBF responses, which depended on distance to the injection site. Near the injector, we observed a decrease in the visually evoked BOLD and CBF responses and an increase in the baseline. The region further away from the injection site was characterized by increased visually evoked BOLD and CBF responses, without affecting the baseline of fMRI signals. These hemodynamic responses to visual modulation after ACh injection qualitatively reflect the changes in neural activity, suggesting that ACh and its metabolites do not cause large changes to the correspondence between fMRI signals and the neurophysiological responses.

The decrease in the stimulus-evoked BOLD and CBF responses in the near region indicate that the [dHb] increased during the ACh injection compared with the preinjection response. A decrease in BOLD and CBF modulation occur when the O_2 consumption stays the same or decreases by a smaller amount than the reduction in inflow (72); the reduced neural activity suggests that there is also a decrease in metabolic demand. The increases in modulation of the hemodynamic and neural responses in the region far from the injector suggest an increased metabolic demand due to the increased neural activity, which might be due to the activation of nAChRs caused by Ch (45). The ACh- and Ch-induced changes to BOLD, CBF, and neural activity are in the same direction, suggesting qualitatively that neurovascular coupling is preserved. Further studies are needed to determine quantitative relationships between neural activity, BOLD, and CBF and to determine the impact of ACh and Ch on the neural population activity and fMRI responses in behaving animals.

The increase in the baseline of the BOLD and CBF near the injector may be due to an increase in blood flow due to vasodilation as a direct vascular effect of ACh (39, 71). Given that the baseline neural activity did not change, such a vascular effect is likely. Type 5 mAChRs are expressed on the surface of vessels in rodents, and their activation was shown to increase blood flow (73, 74). However, it is still unclear whether this subclass of mAChRs is also expressed on vessels in monkey or human cortex (75). Another possible explanation may be the increased concentration of extracellular GABA resulting from the activation of mAChRs due to the continuous infusion of ACh during the injection period (31, 33, 49). Although an increase in GABA would reduce neural activity and thereby fMRI responses, the increased GABA can also lead to enhanced production of nitric oxide and consequently vasodilation (76). Indeed, this has been demonstrated in optogenetic studies where selective activation of PV-ir interneurons caused vasodilation and increased the CBF (76–78). The absence of changes to the baseline further away from the injector also argues for a possible effect in this region of Ch, which is not known to have direct effects on the vasculature. Further studies are needed to elucidate the exact contributions of these mechanisms.

The reduction of stimulus-evoked neural activity, BOLD, and CBF nearby the injector suggest a reduction of energy use after stimulation as a result of the reduced neural activity. Similarly, the increase in stimulus-induced BOLD, CBF, and neural activity suggests an increase in energy use upon stimulation. Although these are relative changes, CBF changes can be quantified in absolute terms, and $CMRO_2$ changes can be measured by using the calibrated BOLD method (79). Baseline values are less accessible with the techniques we used and under this experimental paradigm. Although BOLD fMRI is a relative metric, baseline CBF can be quantified. What we called "baseline changes" here were the slow (stimulus-independent) changes right after ACh injection. However, it would be possible to measure the slow (resting-state) fluctuations in neural activity, BOLD, and CBF in the presence and absence of ACh, which could provide information about the nature of these slow changes, their neural and vascular contributions, and their relation to neuromodulation. However, this was beyond the scope of this study, but would be interesting for further study.

Local and Global Cholinergic Influence. Much of what we know about the impact of cholinergic neuromodulation on the fMRI and neural activity has emerged from studies using electrical stimulation of BFB or using pharmacology to systemically increase the concentration of ACh (22, 23, 74, 80, 81). A systemic increase in the level of ACh is known to up-regulate neural responses to stimuli in the somatosensory (26), auditory (27), and visual cortices (16, 52, 81). However, whether the reported changes are purely due to a cholinergic effect or due to the generation of recurrent loops instantiated by the activation AChRs in multiple brain areas is largely unknown.

The two profiles of fMRI and neural activity show that ACh can act on local cortical circuits in V1, with responses varying considerably depending on the features of the circuits. The distance from where the neuromodulator is released, its concentration and kinetics (60), location (19, 20), distribution, and density of AChRs (32, 33) are factors that play a role in ACh's effects and should be taken into account before inferences can be made about cholinergic effects in cortical sensory areas. Furthermore, similar aspects to those of cholinergic neuromodulation may also apply to other neuromodulators, given that neuromodulators can mediate activity locally or through long-range anatomical connections with other brain areas, or a combination of both. Therefore, our findings highlight the importance of making a distinction between these mechanisms of action to improve the interpretation of fMRI signals.

ACh Increases the SNR of Neural Responses. It has been shown that stimulus encoding improves under influence of cholinergic neuromodulation (15, 38), and our results are in good agreement with this idea, as we found an increase in SNR in the γ and MUA bands near the injection site. This improved efficiency has been linked to the activation of mAChRs expressed in the superficial cortical layers (31, 32). ACh has also been shown to play an important role in gain modulation, as it is known to enhance the activity from stronger inputs while decreasing the weaker inputs, leading to an increase in SNR and promoting the readout of task-related information (9, 15, 38). Our results show that far from the injection site, the SNR decreases in both γ bands. This might be due to the effects induced by the diffusion of Ch, given that it activates α7-nAChRs, which is known to decrease disinhibition (45, 82) and to increase neural activity at different rates (44, 67). How this affects behavior needs to be tested in awake animals.

Limitations. A limitation of our study is that the combined electrophysiology and BOLD data and the CBF and the ECoG data were collected in different experimental sessions/animals. This

was due to the technical difficulty of the experiments and the long duration of the injection experiment. Hardware issues limited the techniques that could be combined; for instance, the transmit radiofrequency (RF) coil and phased array needed for CBF measurement was not compatible with simultaneous electrophysiological recording, and the presence of electrodes reduces image SNR and creates artifacts, precluding accurate CBF measurement. Also, the ECoG grid was not compatible with simultaneous MRI. Although average traces allow qualitative comparisons of neural activity and BOLD and CBF data, the data do not support direct quantitative comparison. The interindividual variation between animals (83) also limits the quantitative inferences that can be made, and further combined experiments would be needed to address such questions.

Another possible limitation might be the layer specificity of our neurophysiological recordings and pharmacological manipulations. The injections and recordings performed by using the μECoG arrays were confined to upper cortical layers, known to express mAChRs and to most accurately encode visual information (41). Although we cannot assign a specific laminar origin to the injection and recording sites in the concurrent neurophysiology and fMRI experiments, we believe that our recordings and injections were mostly performed in superficial layers (e.g., II/III) based on the following points: First, the electrode and the injector formed a single unit and were inserted by using a microdrive that allowed us to determine the depth of the electrode penetration. Additionally, electrode insertion was done slowly under visual and auditory guidance. The electrode has to traverse layers II/III, which are layers with strong stimulus activity (84). Given the difficulty of our experiments and the long duration of the injection trials, we usually recorded from a single site (one electrode penetration) per day.

We recorded all experiments under general anesthesia, and we do not foresee opportunities to perform similar manipulations in alert monkeys in the near future. However, our anesthesia protocol targets μ-opioid receptors which are highly expressed in basal ganglia and thalamus, especially in regions related to motor function and pain, but regions associated with cognition (e.g., the ventral tegmental area, substantia nigra, and frontal regions) have low densities of μ-opioid receptors (85). A study from our laboratory that compared results obtained in anesthetized monkeys with results from alert monkeys found that the neurovascular coupling was relatively unaffected by this anesthesia protocol (1, 4), and a subsequent study reported that the face-processing network was largely unchanged under this anesthesia regimen (86). Therefore, it is unlikely that the anesthesia regimen we used had a major influence on the profiles of neural and hemodynamic responses reported here. Anesthetized animals are, of course, not affected by changes in behavioral state, and although this poses an advantage by allowing us to assess effects of cholinergic neuromodulation without the need to take behavioral parameters or the effect of other neuromodulators into account, it is a limitation in the sense that it does not allow us to relate our results directly to behavior.

Conclusions

Our results provide a comprehensive account of the effects of locally applied ACh on neural and hemodynamic responses in the macaque visual cortex. Our results show that local manipulations of cholinergic neuromodulation elicit changes in neural and fMRI activity that differ depending on the distance from the injector and also from changes reported during systemic manipulation of ACh (22, 23, 74), where increases in fMRI and neural responses were observed. This illustrates the difference between local and global neuromodulatory effects of ACh on neurovascular coupling and shows that it is essential to understand the specific profiles of neural and metabolic activity in any circuit of interest. The combination of BOLD with CBF and/or CBV measurements as well as with electrophysiology can help resolve some of these complexities and can deepen our understanding of the physiological function and pathologies involving the cholinergic system. A better understanding of the effects of neuromodulators on the BOLD response may improve the interpretation of fMRI studies such as studies of reward and attention, etc., where neuromodulation plays a role.

Materials and Methods

Subjects and Ethical Statement. We collected data from eight rhesus monkeys (*Macaca mulatta*, seven males and one female), 5–9 y old weighing 8–12 kg. All experimental procedures were carried out under anesthesia and were approved by the local authorities (Regierungspräsidium, Tübingen, Germany, Project nos. KY01-07 and KY04-16). Experiments were in full compliance with the guidelines of the European Community for the care and use of laboratory animals (EUVD 86/609/EEC).

MRI Scanning. We acquired BOLD signals and fCBF using a vertical 4.7 Tesla Bruker BioSpec scanner with 40-cm-diameter bore (Bruker BioSpin GmbH). We performed 15 BOLD experiments and 7 CBF experiments. For the BOLD experiments, we used a custom-built RF surface coil with an inner diameter of 30 mm as transceiver, positioned around the recording chamber. For BOLD experiments we used an 8-shot Gradient Echo EPI with a field of view (FOV) of 6.4 × 3.2 mm^2, slice thickness of 1 mm, an in-plane resolution of 0.25 × 0.25 mm^2, matrix 128 × 256, and receiver bandwidth (BW) 100 kHz. Echo time (TE) and repetition time (TR) were 18 and 500 ms, respectively, with a flip angle of 30°. Each experimental session consisted of 592 volumes. To ensure good homogeneity of the magnetic field, we used FASTMAP to shim over a volume of 12 mm^3 (87) positioned in the area of the electrode tip. For fCBF measurements, we used a volume coil to transmit in combination with a custom-built two-channel receive phased array (88). For perfusion imaging, a flow-sensitive alternating inversion recovery (FAIR) sequence (89) was used with alternating slice-selective and nonselective inversion pulses (13–15 ms hyperbolic secant pulse). After an inversion time (TI) of 1,300 ms, a single-slice, single-shot EPI image was collected. FOV was 64 × 64 mm^2, resolution 1 × 1 mm^2, slice thickness 3 mm, receiver BW 100 kHz, and TE/TR 11.5/3,000 ms. Anatomical reference scans were T_2-weighted scans (RARE) with a FOV of 64 × 64 mm^2, slice thickness 1 mm, resolution 0.1 × 0.1 mm^2, and TE/TR 46.8/4,800 ms.

Single-Electrode Neurophysiology. Single-electrode recordings were made simultaneously with BOLD fMRI. The electrodes were custom-built and consisted of glass-coated platinum-iridium wires. The tip of the wires was custom-ground with a 50° angle (3). The amplifiers for the single-electrode neurophysiology recordings were custom-built and consisted of an analog compensation mechanism for the noise induced by gradient switching and RF pulses of the scanner. The details of the methods for interference compensation and signal conditioning are given elsewhere (1, 4, 90). The interference-compensated signal was then read in by an analog–digital (AD) converter with 16-bit resolution (National Instruments). The AD converter was linked directly to a PC running a real-time operating system (QNX). Since hardware-based gradient noise compensation is incomplete, additional software-based cleaning of scanner-induced interference was done with custom-written code based on principal component analysis in MATLAB (The MathWorks; for details, see refs. 1 and 91).

μECoG Arrays. We custom-designed a μECoG array to record field potentials from macaque visual cortex (NeuroNexus Technologies, Inc.). The array was microfabricated on a very thin polyimide film (20 μm) with electrode sites of 50-μm diameter spaced 500 μm apart on a 4 × 8 grid (i.e., 1.5 × 4.0 mm^2 rectangular grid). We acutely implanted the μECoG arrays on the surface of V1. For this, we first performed small skull trepanations (6 mm diameter) using stereotaxic coordinates in each monkey. Subsequently, we carefully dissected the meninges layer-wise under the microscope (Zeiss Opmi MDU/S5) to expose the surface of V1 (Fig. 4*A*). The injector was attached to a manual micromanipulator (Narashige Group), which kept the probe in the desired position throughout the experiment. We measured the impedance of the electrode sites before and during the experiments, which ranged from 400 to 600 kΩ. The signals were amplified and filtered into a band of 1 Hz to 8 kHz using a multichannel-processor amplifier system (Alpha-Omega Engineering) and then digitized at 20.833 kHz with a 16-bit resolution ADC converter (National Instruments). LFPs were extracted by bandpass-filtering the signals and downsampling in two steps: (*i*) first to a sampling rate of 1.5 kHz by using a fourth-order Butterworth filter (500-Hz cutoff edge); and (*ii*) to 500 Hz by using a Kaiser window between 1 and 150 Hz, with a (1-Hz) transition band and stopband attenuation of 60 dB. This two-step procedure was computationally more efficient

than a single filtering operation to the final sampling rate. The sharp second filter was used to avoid aliasing, without requiring a higher sampling rate attributable to a broad filter transition band, which would have increased the computational cost of all subsequent operations.

Pharmacology. The injectors were custom-designed and consisted of fused-silica capillary tubing with an inner diameter of 20 μm. For the experiments that were conducted in the MRI scanner, electrode and injector formed one unit to assure placement of both at the same depth (the distance from the injector tip to the electrode was held constant at <1 mm). We used the same injectors for the μECoG experiments, but here the μECoG array and the injector were placed independently following dissection of the dura mater.

Before the experiment, we attached the injector to the infusion line that was directly connected to our pressure-operated injection system (34). This line was monitored by high-precision flow meters (Sensirion) controlling the exact applied volume and the actual flow. We used a 1 mM solution of ACh to induce cholinergic effects in a sufficiently large cortical area to be detectable by fMRI (final injected volume 25 μL). We determined the optimal concentration and flow rate for our ACh injection by following the time course of ACh and Ch during the entire experiment using intracortical sampling of EBF and neurochemistry (for details, see *SI Appendix*, Fig. S1). This was done to establish the effects of ACh in the near region while following the effects caused by ACh's metabolism (21). The concentration that we used in our current study was optimized to account for the very rapid conversion of ACh to Ch by AChE. We observed that at a concentration of 1 mM, the level of ACh rapidly increased, followed by an increase in the Ch level. This was essential in our study, given that a slow and sustained increase in the ACh levels (using lower concentrations) would have led to a rapid degradation of ACh into Ch in the near region (62, 92). Although the concentration that we injected in V1 was higher than the physiological concentrations reported in rodents (0.1–100 μM; ref. 93), the concentration used in our study was lower than the concentrations used in previous iontophoretic in vivo studies and in vitro studies (15, 68, 94) and was the lowest concentration that induced changes to the fMRI signals.

We applied the ACh after the fourth repetition of the visual stimulus, and the injection lasted 8 min (injection period). The pressure-operated injection system maintained a constant flow during the injection period (34). The ACh solution was freshly prepared by using ACh-hydrochloride in ACSF. The ACSF consisted of NaCl (148.19 mM), KCl (3.0 mM), $CaCl_2$ (1.40 mM), $MgCl_2$ (0.80 mM), Na_2HPO_4 (0.80 mM), and NaH_2PO_4 (0.20 mM). The pH was adjusted with NaOH to 7.25. Finally, drug-free ACSF was used for the control condition (11). All chemicals were purchased from Sigma-Aldrich (Schnelldorf).

MRI Data Analysis. All data-analysis procedures were implemented in MATLAB. We defined two ROIs that consisted of gray matter in V1, near to (NEAR) and further from (FAR) the injector: (*i*) ROI_{NEAR} was characterized by the gray matter surrounding the injector tip and electrode (2 mm diameter); and (*ii*) ROI_{FAR} consisted of gray matter further away from the injector (3–5 mm; Fig. 1*B*). For each experiment, two sessions were acquired: An 8-min localizer scan preceding the injection scan was used to identify the voxels showing reliable visually induced modulation in the Sdefined ROIs (Fig. 1*B* shows the NEAR and FAR ROIs). We used a boxcar convolved with a hemodynamic-response function (γ variant function) as regressor to detect visually induced modulation. We used this regressor to calculate the correlation coefficient for every voxel. All voxels showing robust visually induced modulation ($P < 0.02$) were used for the pharmaco-based MRI scan. The voxels identified in the localizer scan were then monitored during the injection scan (39.5 min) and evaluated for ACh-induced effects. We high-pass-filtered (cutoff frequency 0.0005 Hz) the BOLD and CBF time courses to separate the visually induced modulation from the baseline changes. The time course of the visually induced modulation was then calculated by subtracting the image intensity during the OFF periods from the ON periods and dividing by the OFF period (multiplied by 100 to obtain percent). Baseline changes were computed by taking the image intensity in each period without visual stimulation and dividing this by the mean preinjection baseline and converting to a percentage. Mean ACh-induced changes in baseline and modulation were calculated during the injection period (shaded gray area in all figures) and normalized to the preinjection period.

Electrophysiology Data Analysis. To analyze the electrophysiology data, we used a 1-s nonoverlapping window to calculate the PSD of different frequency bands. We extracted the LFPs and MUA by band-pass filtering the signals using custom-written MATLAB routines. Forward and backward filtering was used to eliminate phase shifts introduced by the filters. The boundaries for each frequency band were estimated by quantifying amplitude covariations across LFP frequencies. This procedure involved computing the signal and noise correlations to distinguish LFP frequencies sharing common neural properties (for details, see refs. 34 and 95).

To better visualize the power changes due to the pharmacological intervention, we computed the visually induced modulation for each frequency band in the same way as described in *MRI Data Analysis*. The SNR was computed as described (10). Briefly, we calculated the SNR as the logarithm of the power ratio between the signal (during periods with sensory stimulation) and the noise (periods with no sensory stimulation):

$$SNR_{dB} = 10log_{10}\left(\frac{Signal\ Power}{Noise\ Power}\right),$$

where the SNR takes changes in amplitude as well as in variability into account, and thus can be thought of as a measure of coding efficiency (38).

ACKNOWLEDGMENTS. We thank Deniz Ipek, Mirko Lindig, Thomas Steudel, Mark Augath, and Axel Oeltermann for their technical assistance; and Ulrike Passlack for her help during anesthesia. This work was supported by the Max Planck Society and DFG Grant ZA990/1-1 (to D.Z.).

1. Logothetis NK, Pauls J, Augath M, Trinath T, Oeltermann A (2001) Neurophysiological investigation of the basis of the fMRI signal. *Nature* 412:150–157.
2. Logothetis NK (2008) What we can do and what we cannot do with fMRI. *Nature* 453:869–878.
3. Rauch A, Rainer G, Augath M, Oeltermann A, Logothetis NK (2008) Pharmacological MRI combined with electrophysiology in non-human primates: Effects of lidocaine on primary visual cortex. *Neuroimage* 40:590–600.
4. Goense JB, Logothetis NK (2008) Neurophysiology of the BOLD fMRI signal in awake monkeys. *Curr Biol* 18:631–640.
5. Magri C, Schridde U, Murayama Y, Panzeri S, Logothetis NK (2012) The amplitude and timing of the BOLD signal reflects the relationship between local field potential power at different frequencies. *J Neurosci* 32:1395–1407.
6. Boynton GM (2011) Spikes, BOLD, attention, and awareness: A comparison of electrophysiological and fMRI signals in V1. *J Vis* 11:12.
7. Maier A, et al. (2008) Divergence of fMRI and neural signals in V1 during perceptual suppression in the awake monkey. *Nat Neurosci* 11:1193–1200.
8. Dayan P (2012) Twenty-five lessons from computational neuromodulation. *Neuron* 76:240–256.
9. Yu AJ, Dayan P (2005) Uncertainty, neuromodulation, and attention. *Neuron* 46:681–692.
10. Zaldivar D, Rauch A, Whittingstall K, Logothetis NK, Goense J (2014) Dopamine-induced dissociation of BOLD and neural activity in macaque visual cortex. *Curr Biol* 24:2805–2811.
11. Rauch A, Rainer G, Logothetis NK (2008) The effect of a serotonin-induced dissociation between spiking and perisynaptic activity on BOLD functional MRI. *Proc Natl Acad Sci USA* 105:6759–6764.
12. Thiele A, Bellgrove MA (2018) Neuromodulation of attention. *Neuron* 97:769–785.
13. Mitterschiffthaler MT, Ettinger U, Mehta MA, Mataix-Cols D, Williams SC (2006) Applications of functional magnetic resonance imaging in psychiatry. *J Magn Reson Imaging* 23:851–861.
14. Deco G, Thiele A (2009) Attention: Oscillations and neuropharmacology. *Eur J Neurosci* 30:347–354.
15. Herrero JL, et al. (2008) Acetylcholine contributes through muscarinic receptors to attentional modulation in V1. *Nature* 454:1110–1114.
16. Pinto L, et al. (2013) Fast modulation of visual perception by basal forebrain cholinergic neurons. *Nat Neurosci* 16:1857–1863.
17. Newman EL, Gupta K, Climer JR, Monaghan CK, Hasselmo ME (2012) Cholinergic modulation of cognitive processing: Insights drawn from computational models. *Front Behav Neurosci* 6:24.
18. Mesulam MM, Mufson EJ, Levey AI, Wainer BH (1983) Cholinergic innervation of cortex by the basal forebrain: Cytochemistry and cortical connections of the septal area, diagonal band nuclei, nucleus basalis (substantia innominata), and hypothalamus in the rhesus monkey. *J Comp Neurol* 214:170–197.
19. Disney AA, Domakonda KV, Aoki C (2006) Differential expression of muscarinic acetylcholine receptors across excitatory and inhibitory cells in visual cortical areas V1 and V2 of the macaque monkey. *J Comp Neurol* 499:49–63.
20. Zilles K, Palomero-Gallagher N (2017) Multiple transmitter receptors in regions and layers of the human cerebral cortex. *Front Neuroanat* 11:78.
21. Coppola JJ, Ward NJ, Jadi MP, Disney AA (2016) Modulatory compartments in cortex and local regulation of cholinergic tone. *J Physiol Paris* 110:3–9.
22. Lecrux C, et al. (2017) Impact of altered cholinergic tones on the neurovascular coupling response to whisker stimulation. *J Neurosci* 37:1518–1531.
23. Dauphin F, Lacombe P, Sercombe R, Hamel E, Seylaz J (1991) Hypercapnia and stimulation of the substantia innominata increase rat frontal cortical blood flow by different cholinergic mechanisms. *Brain Res* 553:75–83.
24. Sato A, Sato Y, Uchida S (2001) Regulation of regional cerebral blood flow by cholinergic fibers originating in the basal forebrain. *Int J Dev Neurosci* 19:327–337.
25. Biesold D, Inanami O, Sato A, Sato Y (1989) Stimulation of the nucleus basalis of Meynert increases cerebral cortical blood flow in rats. *Neurosci Lett* 98:39–44.

26. Tremblay N, Warren RA, Dykes RW (1990) Electrophysiological studies of acetylcholine and the role of the basal forebrain in the somatosensory cortex of the cat. II. Cortical neurons excited by somatic stimuli. *J Neurophysiol* 64:1212–1222.
27. Metherate R, Ashe JH (1993) Nucleus basalis stimulation facilitates thalamocortical synaptic transmission in the rat auditory cortex. *Synapse* 14:132–143.
28. Turchi J, et al. (2018) The basal forebrain regulates global resting-state fMRI fluctuations. *Neuron* 97:940–952.e4.
29. Hasselmo ME, Anderson BP, Bower JM (1992) Cholinergic modulation of cortical associative memory function. *J Neurophysiol* 67:1230–1246.
30. Disney AA, Alasady HA, Reynolds JH (2014) Muscarinic acetylcholine receptors are expressed by most parvalbumin-immunoreactive neurons in area MT of the macaque. *Brain Behav* 4:431–445.
31. Disney AA, Aoki C (2008) Muscarinic acetylcholine receptors in macaque V1 are most frequently expressed by parvalbumin-immunoreactive neurons. *J Comp Neurol* 507:1748–1762.
32. Disney AA, Aoki C, Hawken MJ (2007) Gain modulation by nicotine in macaque v1. *Neuron* 56:701–713.
33. Disney AA, Aoki C, Hawken MJ (2012) Cholinergic suppression of visual responses in primate V1 is mediated by GABAergic inhibition. *J Neurophysiol* 108:1907–1923.
34. Zaldivar D, Logothetis NK, Rauch A, Goense J (2017) Pharmaco-based fMRI and neurophysiology in non-human primates. *Neuromethods* 121:37–66.
35. Buzsáki G, Anastassiou CA, Koch C (2012) The origin of extracellular fields and currents–EEG, ECoG, LFP and spikes. *Nat Rev Neurosci* 13:407–420.
36. Buzsáki G, Kaila K, Raichle M (2007) Inhibition and brain work. *Neuron* 56:771–783.
37. Belitski A, et al. (2008) Low-frequency local field potentials and spikes in primary visual cortex convey independent visual information. *J Neurosci* 28:5696–5709.
38. Minces V, Pinto L, Dan Y, Chiba AA (2017) Cholinergic shaping of neural correlations. *Proc Natl Acad Sci USA* 114:5725–5730.
39. Zappe AC, Uludağ K, Logothetis NK (2008) Direct measurement of oxygen extraction with fMRI using 6% CO2 inhalation. *Magn Reson Imaging* 26:961–967.
40. Goense J, Merkle H, Logothetis NK (2012) High-resolution fMRI reveals laminar differences in neurovascular coupling between positive and negative BOLD responses. *Neuron* 76:629–639.
41. Zaldivar D, Goense J, Lowe SC, Logothetis NK, Panzeri S (2018) Dopamine is signaled by mid-frequency oscillations and boosts output layers visual information in visual cortex. *Curr Biol* 28:224–235 e5.
42. Fukushima M, Saunders RC, Leopold DA, Mishkin M, Averbeck BB (2012) Spontaneous high-gamma band activity reflects functional organization of auditory cortex in the awake macaque. *Neuron* 74:899–910.
43. Ray S, Maunsell JH (2011) Different origins of gamma rhythm and high-gamma activity in macaque visual cortex. *PLoS Biol* 9:e1000610.
44. Albuquerque EX, Pereira EF, Braga MF, Alkondon M (1998) Contribution of nicotinic receptors to the function of synapses in the central nervous system: The action of choline as a selective agonist of alpha 7 receptors. *J Physiol Paris* 92:309–316.
45. Alkondon M, Albuquerque EX (2006) Subtype-specific inhibition of nicotinic acetylcholine receptors by choline: A regulatory pathway. *J Pharmacol Exp Ther* 318:268–275.
46. Zhang X, et al. (2007) Capillary hydrophilic interaction chromatography/mass spectrometry for simultaneous determination of multiple neurotransmitters in primate cerebral cortex. *Rapid Commun Mass Spectrom* 21:3621–3628.
47. Mrzljak L, Levey AI, Goldman-Rakic PS (1993) Association of m1 and m2 muscarinic receptor proteins with asymmetric synapses in the primate cerebral cortex: Morphological evidence for cholinergic modulation of excitatory neurotransmission. *Proc Natl Acad Sci USA* 90:5194–5198.
48. Van Brederode JF, Mulligan KA, Hendrickson AE (1990) Calcium-binding proteins as markers for subpopulations of GABAergic neurons in monkey striate cortex. *J Comp Neurol* 298:1–22.
49. Müller CM, Singer W (1989) Acetylcholine-induced inhibition in the cat visual cortex is mediated by a GABAergic mechanism. *Brain Res* 487:335–342.
50. McCormick DA, Prince DA (1986) Mechanisms of action of acetylcholine in the guinea-pig cerebral cortex in vitro. *J Physiol* 375:169–194.
51. Gil Z, Connors BW, Amitai Y (1997) Differential regulation of neocortical synapses by neuromodulators and activity. *Neuron* 19:679–686.
52. Goard M, Dan Y (2009) Basal forebrain activation enhances cortical coding of natural scenes. *Nat Neurosci* 12:1444–1449.
53. Gulledge AT, Park SB, Kawaguchi Y, Stuart GJ (2007) Heterogeneity of phasic cholinergic signaling in neocortical neurons. *J Neurophysiol* 97:2215–2229.
54. Gonchar Y, Burkhalter A (1997) Three distinct families of GABAergic neurons in rat visual cortex. *Cereb Cortex* 7:347–358.
55. Xiang Z, Huguenard JR, Prince DA (1998) Cholinergic switching within neocortical inhibitory networks. *Science* 281:985–988.
56. Hasselmo ME, Giocomo LM (2006) Cholinergic modulation of cortical function. *J Mol Neurosci* 30:133–135.
57. Smith MA, Kohn A (2008) Spatial and temporal scales of neuronal correlation in primary visual cortex. *J Neurosci* 28:12591–12603.
58. Martin KAC, Roth S, Rusch ES (2014) Superficial layer pyramidal cells communicate heterogeneously between multiple functional domains of cat primary visual cortex. *Nat Commun* 5:5252.
59. Kimura A, Sato A, Takano Y (1990) Stimulation of the nucleus basalis of Meynert does not influence glucose utilization of the cerebral cortex in anesthetized rats. *Neurosci Lett* 119:101–104.
60. Agnati LF, et al. (2006) Volume transmission and wiring transmission from cellular to molecular networks: History and perspectives. *Acta Physiol (Oxf)* 187:329–344.
61. Agnati LF, Zoli M, Strömberg I, Fuxe K (1995) Intercellular communication in the brain: Wiring versus volume transmission. *Neuroscience* 69:711–726.
62. Sarter M, Parikh V, Howe WM (2009) Phasic acetylcholine release and the volume transmission hypothesis: Time to move on. *Nat Rev Neurosci* 10:383–390.
63. Umbriaco D, Watkins KC, Descarries L, Cozzari C, Hartman BK (1994) Ultrastructural and morphometric features of the acetylcholine innervation in adult rat parietal cortex: An electron microscopic study in serial sections. *J Comp Neurol* 348:351–373.
64. Mesulam MM, Geula C (1991) Acetylcholinesterase-rich neurons of the human cerebral cortex: Cytoarchitectonic and ontogenetic patterns of distribution. *J Comp Neurol* 306:193–220.
65. Chakrin LW, Marchbanks RM, Mitchell JF, Whittaker VP (1972) The origin of the acetylcholine released from the surface of the cortex. *J Neurochem* 19:2727–2736.
66. Alkondon M, Pereira EFR, Cortes WS, Maelicke A, Albuquerque EX (1997) Choline is a selective agonist of alpha7 nicotinic acetylcholine receptors in the rat brain neurons. *Eur J Neurosci* 9:2734–2742.
67. Papke RL, Bencherif M, Lippiello P (1996) An evaluation of neuronal nicotinic acetylcholine receptor activation by quaternary nitrogen compounds indicates that choline is selective for the alpha 7 subtype. *Neurosci Lett* 213:201–204.
68. Kimura F, Fukuda M, Tsumoto T (1999) Acetylcholine suppresses the spread of excitation in the visual cortex revealed by optical recording: Possible differential effect depending on the source of input. *Eur J Neurosci* 11:3597–3609.
69. Barker LA, Dowdall MJ, Whittaker VP (1972) Choline metabolism in the cerebral cortex of guinea pigs. Stable-bound acetylcholine. *Biochem J* 130:1063–1075.
70. Magistretti PJ, Allaman I (2015) A cellular perspective on brain energy metabolism and functional imaging. *Neuron* 86:883–901.
71. Sicard KM, Duong TQ (2005) Effects of hypoxia, hyperoxia, and hypercapnia on baseline and stimulus-evoked BOLD, CBF, and CMRO2 in spontaneously breathing animals. *Neuroimage* 25:850–858.
72. Mullinger KJ, Mayhew SD, Bagshaw AP, Bowtell R, Francis ST (2013) Poststimulus undershoots in cerebral blood flow and BOLD fMRI responses are modulated by poststimulus neuronal activity. *Proc Natl Acad Sci USA* 110:13636–13641.
73. Yamada M, et al. (2001) Cholinergic dilation of cerebral blood vessels is abolished in M(5) muscarinic acetylcholine receptor knockout mice. *Proc Natl Acad Sci USA* 98:14096–14101.
74. Elhusseiny A, Hamel E (2000) Muscarinic—but not nicotinic—acetylcholine receptors mediate a nitric oxide-dependent dilation in brain cortical arterioles: A possible role for the M5 receptor subtype. *J Cereb Blood Flow Metab* 20:298–305.
75. Elhusseiny A, Cohen Z, Olivier A, Stanimirović DB, Hamel E (1999) Functional acetylcholine muscarinic receptor subtypes in human brain microcirculation: Identification and cellular localization. *J Cereb Blood Flow Metab* 19:794–802.
76. Uhlirova H, et al. (2016) Cell type specificity of neurovascular coupling in cerebral cortex. *eLife* 5:e14315.
77. Anenberg E, Chan AW, Xie Y, LeDue JM, Murphy TH (2015) Optogenetic stimulation of GABA neurons can decrease local neuronal activity while increasing cortical blood flow. *J Cereb Blood Flow Metab* 35:1579–1586.
78. Perrenoud Q, et al. (2012) Characterization of type I and type II nNOS-expressing interneurons in the barrel cortex of mouse. *Front Neural Circuits* 6:36.
79. Hoge RD, et al. (1999) Linear coupling between cerebral blood flow and oxygen consumption in activated human cortex. *Proc Natl Acad Sci USA* 96:9403–9408.
80. Kosovicheva AA, Sheremata SL, Rokem A, Landau AN, Silver MA (2012) Cholinergic enhancement reduces orientation-specific surround suppression but not visual crowding. *Front Behav Neurosci* 6:61.
81. Rokem A, Silver MA (2010) Cholinergic enhancement augments magnitude and specificity of visual perceptual learning in healthy humans. *Curr Biol* 20:1723–1728.
82. Albuquerque EX, et al. (2000) Neuronal nicotinic receptors in synaptic functions in humans and rats: Physiological and clinical relevance. *Behav Brain Res* 113:131–141.
83. von Pföstl V, et al. (2012) Effects of lactate on the early visual cortex of non-human primates, investigated by pharmaco-MRI and neurochemical analysis. *Neuroimage* 61:98–105.
84. Gur M, Snodderly DM (2008) Physiological differences between neurons in layer 2 and layer 3 of primary visual cortex (V1) of alert macaque monkeys. *J Physiol* 586:2293–2306.
85. Henriksen G, Willoch F (2008) Imaging of opioid receptors in the central nervous system. *Brain* 131:1171–1196.
86. Ku SP, Tolias AS, Logothetis NK, Goense J (2011) fMRI of the face-processing network in the ventral temporal lobe of awake and anesthetized macaques. *Neuron* 70:352–362.
87. Gruetter R (1993) Automatic, localized in vivo adjustment of all first- and second-order shim coils. *Magn Reson Med* 29:804–811.
88. Goense J, Logothetis NK, Merkle H (2010) Flexible, phase-matched, linear receive arrays for high-field MRI in monkeys. *Magn Reson Imaging* 28:1183–1191.
89. Kim SG (1995) Quantification of relative cerebral blood flow change by flow-sensitive alternating inversion recovery (FAIR) technique: Application to functional mapping. *Magn Reson Med* 34:293–301.
90. Oeltermann A, Augath MA, Logothetis NK (2007) Simultaneous recording of neuronal signals and functional NMR imaging. *Magn Reson Imaging* 25:760–774.
91. Logothetis NK (2002) The neural basis of the blood-oxygen-level-dependent functional magnetic resonance imaging signal. *Philos Trans R Soc Lond B Biol Sci* 357:1003–1037.
92. Parikh V, et al. (2004) Rapid assessment of in vivo cholinergic transmission by amperometric detection of changes in extracellular choline levels. *Eur J Neurosci* 20:1545–1554.
93. Noori HR, Fliegel S, Brand I, Spanagel R (2012) The impact of acetylcholinesterase inhibitors on the extracellular acetylcholine concentrations in the adult rat brain: A meta-analysis. *Synapse* 66:893–901.
94. Verhoog MB, et al. (2016) Layer-specific cholinergic control of human and mouse cortical synaptic plasticity. *Nat Commun* 7:12826.
95. Magri C, Mazzoni A, Logothetis NK, Panzeri S (2012) Optimal band separation of extracellular field potentials. *J Neurosci Methods* 210:66–78.